# Electron- and positron-induced ionization of water molecules: Theory versus experiment at the triply differential scale

P. Singh,[1] G. Purohit,[1] C. Champion,[2] and V. Patidar[1]

[1]*Department of Physics, School of Engineering, Sir Padampat Singhania University, Bhatewar, Udaipur 313 601, India*

[2]*Université Bordeaux 1, CNRS/IN2P3, Centre d'Études Nucléaires de Bordeaux Gradignan (CENBG) Chemin du Solarium, BP120, 33175 Gradignan, France*

(Received 10 January 2014; published 26 March 2014)

Triply differential cross sections for electron- and positron-induced ionization of the $3a_1$ orbital of the water molecule are calculated within the second-order distorted-wave Born approximation. In this context, distorted-wave functions are numerically calculated by modeling both the initial and the final channels whereas single-center Slater-type wave functions are used for describing the molecular target. A good agreement with the existing experimental data is observed. Differences in the trends of differential cross sections are observed for the electron- and positron-impact ionization.

DOI: 10.1103/PhysRevA.89.032714 PACS number(s): 34.80.Gs, 34.50.Gb

## I. INTRODUCTION

Charged particle impact ionization is an important fundamental collision process that plays a significant role in many areas as diverse as plasma physics, astrophysics, atmospheric modeling, discharge physics, and radiobiology. In this context, let us note that the water molecule is the third most abundant molecule on Earth and is therefore of great importance in numerous multidisciplinary research fields such as radiobiology where it is commonly used as a surrogate for living matter, the latter being composed of water for about 60% in mass. As an example, energetic and angular distributions resulting from electron-induced collisions with water molecules are commonly used in charged particle track structure codes for modeling the radio-induced damages in biological samples [1]. In addition, the low-energy electrons—abundantly produced in the high-energy radiation and commonly used in radiotherapy treatment planning—have nowadays been clearly identified as of prime importance, in particular since the observation of their crucial role in lethal cellular lesion induction [2]. Under these conditions, the knowledge of the collision dynamics of such low-energy electrons with biological systems remains crucial so as to develop robust numerical models of charged particle tracking in biological matter.

Studying the electron-impact single-ionization process at the most differential scale, namely, the triply differential scale—commonly referred to as $(e, 2e)$ process—has become a powerful tool for investigating the complete dynamics of the collisional process. In this context, advances on the theoretical side have provided much support for the experiments. However, many-body problems still remain unsolved, the simple atomic hydrogen case remaining up to now the solely three-body problem numerically solved [3]. A lot of data are available for the single ionization of simple atomic hydrogen to more complex atomic and molecular targets [4–6]. Besides, more complex processes such as double ionization, simultaneous excitation and ionization, as well as autoionization [7–9] have also been investigated.

In the last decades, numerous theoretical models have been developed to describe the ionization processes at various impact energies and geometries [4–13]. Each of them uses different kinds of approximations and as a result, the experiments play an important role in checking the accuracy of the theoretical approximations in use. In this context, the distorted-wave Born approximation (DWBA) appears as one of the most reliable alternatives for modeling the ionization process of complex many-electron systems such as noble gas targets, and alkali and alkali-earth metals [14,15]. Indeed, the DWBA-produced results in terms of $(e, 2e)$ triply differential cross sections (TDCSs) have shown a reasonably good agreement with the available experimental data (see, for example, Ref. [16]). However, describing the low-energy electron-induced collisions undoubtedly requires several improvements such as the taking account of postcollisional interaction (PCI), the correlation-polarization effect, as well as the electron exchange phenomenon. Once these fine effects are included, the theoretical results have shown better agreement with experiments for various atomic targets [14,15,17,18]. Apart from the aforementioned effects, the second-order approximation has been designated as particularly suitable for describing the low-energy electron-induced collisional processes [19].

In the current study, we report on the calculation of triply differential cross sections for electron- and positron-induced ionization of the $3a_1$ molecular orbital of the $H_2O$ molecule in coplanar symmetric kinematics within the second-order distorted-wave Born approximation (SBA-DWBA) including postcollision interaction (PCI).

In the sequel, we briefly outline the theoretical model and compare our TDCSs to measurements as well as theoretical predictions provided by the MDW (molecular distorted wave) model [20] in coplanar symmetric kinematics for incident electron energies 4, 10, 20, and 40 eV above the ionization potential of the $3a_1$ molecular state. Then, we discuss the role of the postcollision interaction as well as the influence of the projectile charge on the cross-section determination (electron- versus positron-induced ionization).

## II. THEORY

The electron- and positron-induced single-ionization process on the $H_2O$ molecule is expressed as

$$e^-/e^+ + H_2O \rightarrow H_2O^+ + e^- + e^-/e^+. \qquad (1)$$

 

The triply differential cross section in second Born approximation for the ionization process as in Eq. (1) may be written as

$$\frac{d^3\sigma}{d\Omega_1 d\Omega_2 dE_2} = (2\pi)^4 \frac{k_1 k_2}{k_0} \sum_{\text{av}} |f_{B1} + f_{B2}|^2, \qquad (2)$$

where $\boldsymbol{k}_0$, $\boldsymbol{k}_1$, and $\boldsymbol{k}_2$ are the momenta of incident, scattered, and ejected particles, respectively. The elements $d\Omega_1 = \sin\xi_1 d\xi_1 d\phi_1$ and $d\Omega_2 = \sin\xi_2 d\xi_2 d\phi_2$ denote the solid angle for the scattered and the ejected electron, respectively, whereas the energy interval of the ejected electron is represented by $dE_2$. In the coplanar symmetric geometry used here, $\boldsymbol{k}_0$, $\boldsymbol{k}_1$, and $\boldsymbol{k}_2$ are in the same plane ($\phi_1 = 0$ and $\phi_2 = 180^\circ$) while the scattering and ejection angles are taken as equal ($\xi_1 = \xi_2$). The incident electron energy $E_0$ is defined by the relation $E_0 = E_1 + E_2 + V_i$, where $E_1$ and $E_2$ refer to the energies of the two outgoing electrons while $V_i$ denotes the ionization potential of the $3a_1$ orbital of the water molecule. Let us note that Eq. (2) includes a sum over final and average over initial magnetic and spin-state degeneracy.

The first-order term in DWBA is given by

$$f_{B1} = \left\langle \chi_1^{(-)}(\boldsymbol{k}_1,\boldsymbol{r}_1)\chi_2^{(-)}(\boldsymbol{k}_2,\boldsymbol{r}_0)\right| \pm \left(\frac{Z}{r_1} - \frac{1}{|\boldsymbol{r}_1 - \boldsymbol{r}_0|}\right) \times \left|\Psi_i(\boldsymbol{r}_0)\chi_0^{(+)}(\boldsymbol{k}_0,\boldsymbol{r}_1)\right\rangle, \qquad (3)$$

where the symbol $\pm$ takes into account the charge of the projectile ("+" for positron and "–" for electron) while $Z$ refers to the charge of the ionized target (here $Z = 1$).

$\chi_0^{(+)}(\boldsymbol{k}_0,\boldsymbol{r}_1)$ is the distorted-wave function used for describing the incident particle while $\chi_1^{(-)}(\boldsymbol{k}_1,\boldsymbol{r}_1)$ and $\chi_2^{(-)}(\boldsymbol{k}_2,\boldsymbol{r}_0)$ refer to the distorted-wave functions used for the two outgoing particles. $\Psi_i(\boldsymbol{r}_0)$ is the initial bound-state wave function which is approximated as the orientation-averaged molecular wave function for the $3a_1$ orbital of water molecule.

The initial-state distorted waves are generated in the initial-state distorting potential $V$ constituted by the nuclear contribution plus a spherically symmetric approximated interaction between the incident particle and the target electrons, while the final-state distorted waves are obtained in the final-state distorting potential including the nuclear contribution plus a spherically symmetric approximated interaction between the continuum electron and the electrons in the ion field.

The target molecular orbitals are here expressed in terms of Slater-like functions all centered at a common origin, i.e., the heaviest atom, and are written as

$$\Psi_i(\boldsymbol{r}_0) = \sum_{j=1}^{N_i} a_{ij}\phi^{\xi_{ij}}_{n_{ij}l_{ij}m_{ij}}(\boldsymbol{r}), \qquad (4)$$

where $N_i$ is the number of Slater orbitals $\phi^{\xi_{ij}}_{n_{ij}l_{ij}m_{ij}}(r)$ and $a_{ij}$ the weight of each atomic component,

$$\phi^{\xi_{ij}}_{n_{ij}l_{ij}m_{ij}}(\boldsymbol{r}) = R^{\xi_{ij}}_{n_{ij}l_{ij}}(r)Y_{l_{ij}m_{ij}}(\hat{r}), \qquad (5)$$

with the radial part $R^{\xi_{ij}}_{n_{ij}l_{ij}}(r)$ of each atomic orbital given by

$$R^{\xi_{ij}}_{n_{ij}l_{ij}}(r) = \frac{(2\xi_{ij})^{2n_{ij}+1/2}}{\sqrt{2n_{ij}!}} r^{n_{ij}-1}e^{-\xi_{ij}r}. \qquad (6)$$

Let us note that in Eq. (5), $\hat{r}$ designates the solid angle direction.

All the needed parameters and quantum numbers are taken from Ref. [21] and for more details we refer the reader to Refs. [22–26] where the current water target description was used for describing the electron-induced ionization process.

In the current theoretical model, we have expressed the second-order Born term as

$$f_{B2} = \left\langle \chi^{(-)}(\boldsymbol{k}_1,\boldsymbol{r}_1)\chi^{(-)}(\boldsymbol{k}_2,\boldsymbol{r}_0)\right| V G_0^+ V \left|\Psi_i(\boldsymbol{r}_0)\chi_0^{(+)}(\boldsymbol{k}_0,\boldsymbol{r}_1)\right\rangle, \qquad (7)$$

where $G_0^+$ is the Green's function defined by

$$G_0^+ = \frac{1}{E_0 - H + i\varepsilon}, \qquad (8)$$

where $H$ is the Hamiltonian of target defined by the relation $H = -\frac{\nabla^2}{2} \pm (\frac{Z}{r_1} - \frac{1}{|\boldsymbol{r}_1 - \boldsymbol{r}_0|})$, $E_0$ is the incident energy, and $\varepsilon \to 0^+$.

In addition, let us note that the distorted-wave function used for describing the incident particle is generated in the equivalent local ground-state potential of the water molecule while the distorted-wave functions used for modeling the outgoing particles are generated in the equivalent local ground-state potential of the residual ion. Moreover, let us add that all along the current calculations reported here we have made a careful check to ensure that the cross sections converge satisfactorily. Finally, let us note that the spin-averaged static-exchange potential of Furness and McCarthy [27] as modified by Riley and Truhlar [28] has been used for the case of electron-induced ionization; however, the distorted waves for the positron-impact case have been generated in the static potential of the target. We have included PCI in our DWBA calculations using the Ward-Macek factor ($M_{ee}$) [29]. The $M_{ee}$ is a multiplicative factor to include the postcollision interaction in a simple way and is defined as

$$M_{ee} = N_{ee}|{}_1F_1(-i\lambda_3, 1, -2k_3 r_{3\text{ave}})|^2, \qquad (9)$$

where

$$N_{ee} = \frac{\gamma}{e^\gamma - 1} \quad \text{with} \quad \gamma = -\frac{2\pi}{|k_1 - k_2|},$$
$$\lambda_3 = -\frac{1}{|k_1 - k_2|}, \qquad (10)$$
$$r_{3\text{ave}} = \frac{\pi^2}{16\varepsilon}\left(1 + \frac{0.627}{\pi}\sqrt{\varepsilon}\ln\varepsilon\right)^2.$$

Finally, the TDCSs including PCI are given by

$$\frac{d^3\sigma}{d\Omega_1 d\Omega_2 dE_2} = M_{ee}(2\pi)^4 \frac{k_1 k_2}{k_0} \sum_{\text{av}} |f_{B1} + f_{B2}|^2. \qquad (11)$$

## III. RESULTS AND DISCUSSION

The TDCS calculations have been performed in doubly symmetric coplanar kinematics, i.e., with equal outgoing electron energies and polar angles, namely, $E_1 = E_2$ and $\xi_1 = \xi_2 = \xi$ at several incident energies, namely, 4, 10, 20, and 40 eV above the ionization potential (IP) of the $3a_1$ molecular state ($V_i \sim 15$ eV) of the water molecule.

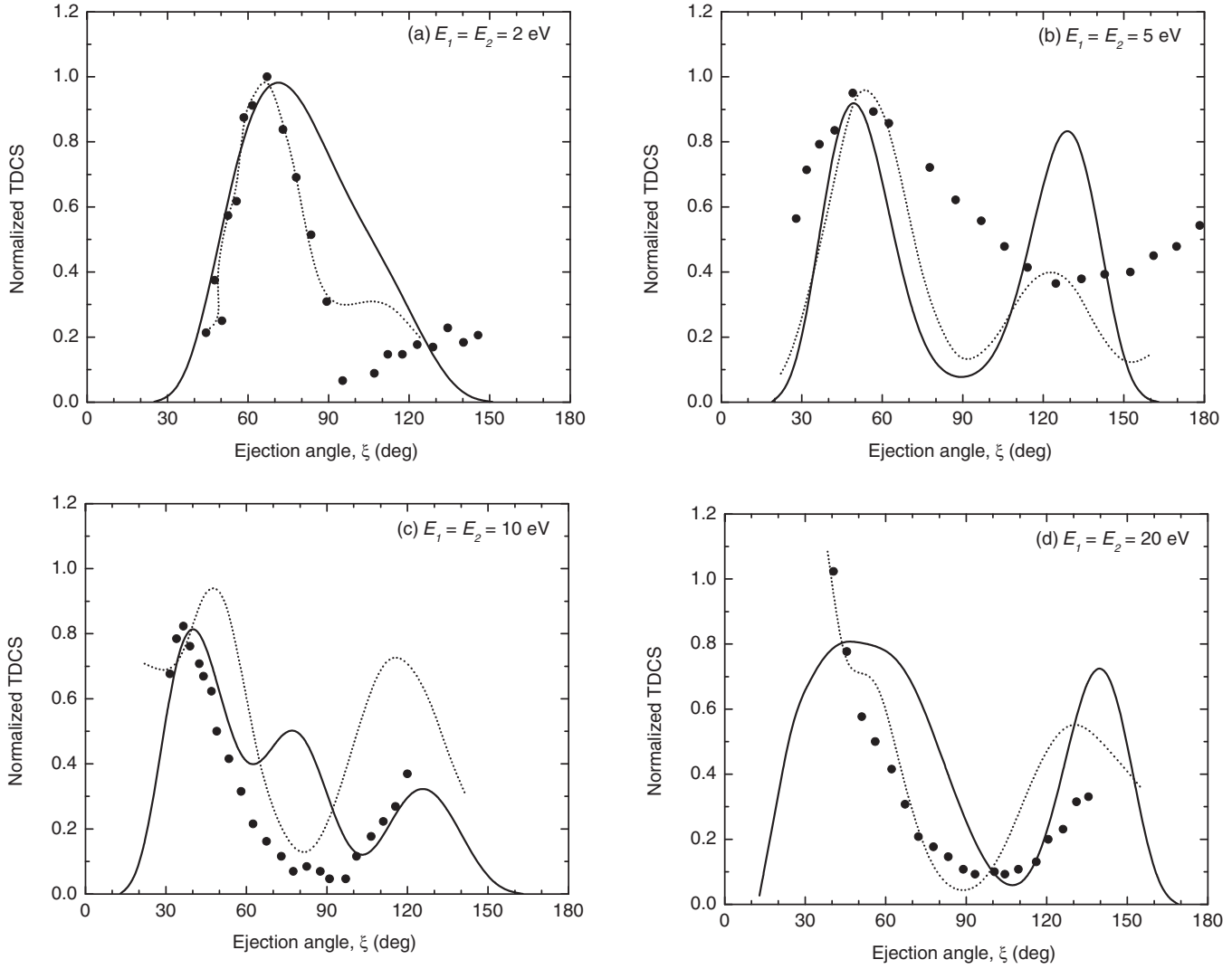


FIG. 1. Triply differential cross sections for the electron-impact ionization of the $3a_1$ molecular state of the water molecule in coplanar symmetric kinematics (i.e., $\phi_1 = 0$, $\phi_2 = 180^\circ$, and $\xi_1 = \xi_2 = \xi$) at several incident electron energies: 4 eV (a), 10 eV (b), 20 eV (c), and 40 eV (d) above the ionization potential (IP $\sim$ 15 eV). The energies of the two outgoing electrons are shown on the respective plots. The solid line represents the second Born distorted-wave Born approximation while the dotted line refers to the molecular distorted wave (MDW) approximation [20]. The experimental (solid circles) and theoretical data have been both independently normalized to unity.

The TDCSs for electron-induced ionization of the water molecule are reported in Fig. 1 as a function of the ejection angle $\xi$. The solid line represents the DWBA calculations including the second-order term (SBA) with postcollision interaction (PCI). We compare our results with the recent measurements of Nixon *et al*. (solid circles) as well as the theoretical predictions provided by the MDW model (dotted line) both taken from Ref. [20]. All the theoretical and experimental data are independently normalized. In all the cases reported in Fig. 1, we observe that the experimental data show a strong peak at forward-scattering angles ($\xi < 90^\circ$) and a small one at backward-scattering angles ($\xi > 90^\circ$). The coplanar differential cross section exhibits a forward peak and a backward peak due to single electron-electron binary collision and double-scattering mechanism, respectively [30]. Besides, we note that the forward peak shifts towards a lower value of ejection angle as the incident electron energy increases from 4 eV above IP to 40 eV above IP. On the theoretical front, a similar trend is observed with the current second-order Born calculations except in the case of incident electron energy 4 eV above IP [Fig. 1(a)]. A reasonable agreement may be observed between our theoretical predictions and the available experimental data, even considering some discrepancies in terms of magnitude as well as position for the forward- and backward-scattering peaks. At incident electron energy 4 eV above IP [Fig. 1(a)] our SBA-DWBA calculations produce a forward-scattering peak at the ejection angle $\xi \approx 70^\circ$, i.e., slightly shifted—as well as enlarged—in comparison to the experimental one, located at $\xi \approx 66^\circ$. However, the small backward-scattering peak observed experimentally is not reproduced in our current SBA-DWBA calculations. In Fig. 1(b), we compare our SBA-DWBA calculations to the available experimental data at the incident electron energy 10 eV above IP. A two-peak structure is theoretically observed with forward- and backward-scattering peaks located at ejection angles $\xi \approx 49^\circ$ and $\xi \approx 128^\circ$, respectively. Some

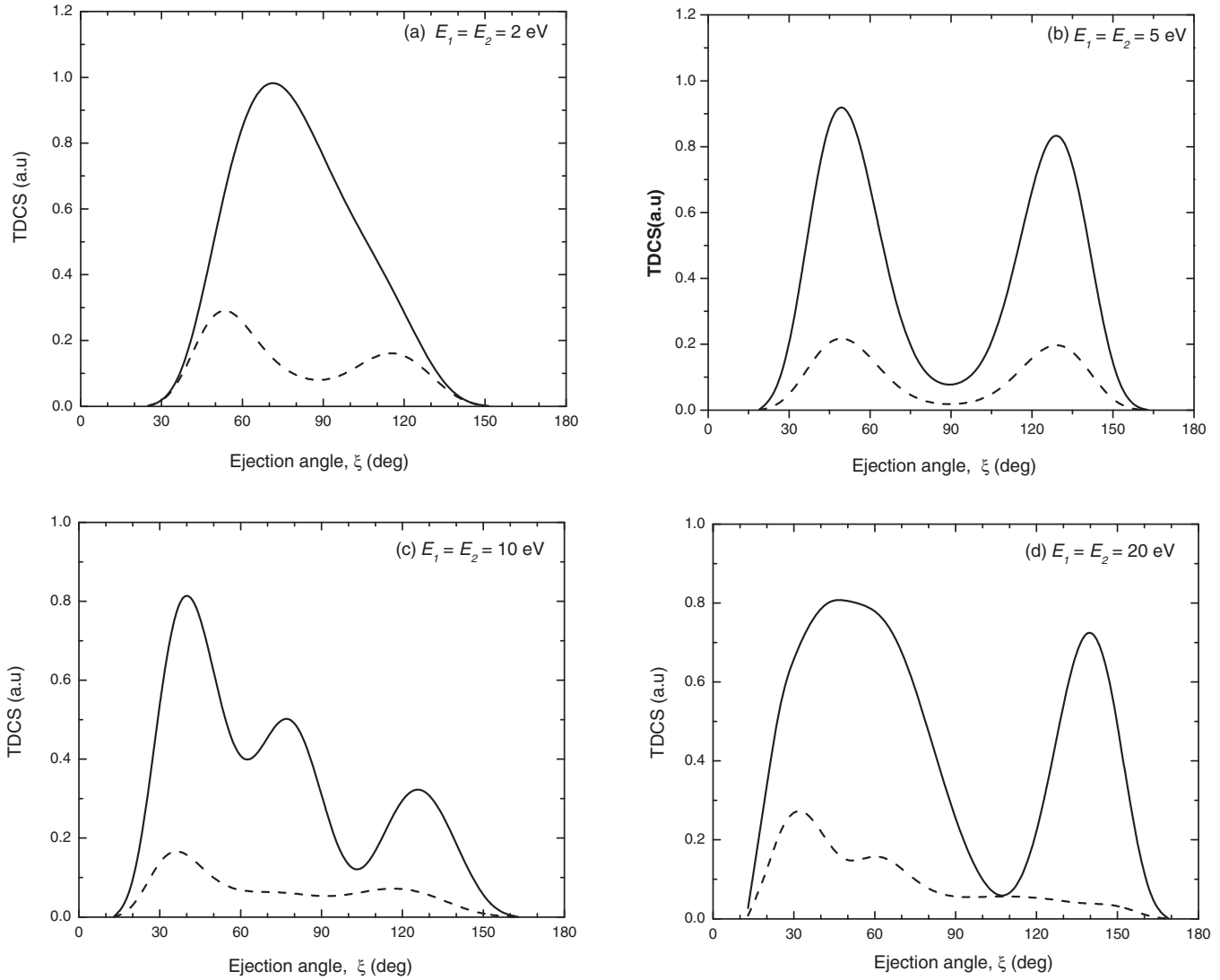


FIG. 2. Triply differential cross sections for electron- and positron-impact ionization of the $3a_1$ state of the water molecule in coplanar symmetric kinematics (i.e., $\phi_1 = 0$, $\phi_2 = 180^\circ$, and $\xi_1 = \xi_2 = \xi$) at several incident electron energies: 4 eV (a), 10 eV (b), 20 eV (c), and 40 eV (d) above the ionization potential (IP $\sim$ 15 eV). The energies of the two outgoing electrons are shown on the respective plots. The solid line represents the electron-impact ionization TDCSs while the dashed line refers to the positron ones.

degree of agreement is observed with the experimental data, in particular in the forward-peak region since the observation also reports a forward peak located around $\xi \approx 49^\circ$. On the contrary, the experimental backward-scattering peak appears as shifted towards a higher ejection angle value, namely, around $\xi \approx 180^\circ$. Regarding now the TDCS profile for the ionization of the $3a_1$ molecular state of the water molecule at the incident electron energy 20 eV above IP in the present second Born approximation [Fig. 1(c)], it is interesting to note that a three-peak structure is then observed pointing out an additional intermediate peak observed at $\xi \approx 77^\circ$, i.e., located between the forward and backward peaks sited at $\xi \approx 40^\circ$ and $\xi \approx 126^\circ$, respectively. Under these conditions, the SBA predictions exhibit a reasonable agreement with the experimental data, the latter showing a (very) small intermediate peak around $\xi \approx 82^\circ$ and forward and backward peaks located at $\xi \approx 36^\circ$ and $\xi \approx 120^\circ$, respectively. At the incident electron energy 40 eV above IP [Fig. 1(d)], the experimental TDCSs do not show a clear two-peak structure since they exhibit a continuous increase below the ejection angle $\xi \approx 60^\circ$ and beyond ejection angle $\xi \approx 120^\circ$ (the peaks may be out of the detector ranges). On the contrary, our SBA calculations clearly provide a two-peak structure with, in particular, a backward peak at $\xi \approx 140^\circ$ and a broad forward peak at $\xi \approx 50^\circ$; the TDCSs exhibit—as expected—a decrease in the forward ($\xi \approx 0^\circ$) and backward directions ($\xi \approx 180^\circ$) due to postcollision interaction (PCI).

To conclude, the current SBA-DWBA predictions in terms of TDCSs have here shown relevant features—from one- to three-peak structures—in reasonable agreement ($\approx$75%) with the experiment, pointing out also significant differences in the low-incident energy regime. Besides, in comparison to the MDW results taken from Ref. [20] (dotted curves in Fig. 1), we observe that both the calculations reproduce a two-peak structure at incident electron energy 10 eV above IP exhibiting, in particular, a good agreement in regards to the position of

the forward-scattering peaks. However, discrepancies in terms of magnitude of the backward-scattering peak are noticeable in our SBA calculations and MDW results at incident electron energy 10 eV above IP [Fig. 1(b)]. The MDW calculations show good agreement with the experimental data in the forward-peak region and also produce a smaller backward peak at the incident electron energy 4 eV above IP [Fig. 1(a)]; however, the position of the backward-scattering peak does not match with the experimental data. Present SBA calculations are able to produce only a broad forward peak at this energy. SBA calculations show improved agreement with the experimental data in the forward- and backward-peak regions at the incident electron energy 20 eV above IP [Fig. 1(c)]; however, they also exhibit an intermediate peak, which is not observed in the MDW calculations. At incident electron energy 40 eV above IP [Fig. 1(d)], the disagreement between the two sets of calculations is more important since the MDW calculations well reproduce the experimental observation, namely, a continuous increase of the TDCSs below an ejection angle $\xi \approx 60^\circ$, contrary to our theoretical SBA-DWBA predictions, which clearly exhibit a forward peak around $\xi \approx 50^\circ$ and then negligible TDCSs in the forward direction ($\xi \approx 0^\circ$), as expected due to the inclusion of the PCI effect into our calculations.

In Fig. 2, we report on the comparison between the electron- and positron-induced coplanar symmetric ionization. Differential cross sections are here again calculated at incident particle energies 4, 10, 20, and 40 eV above the ionization potential of the $3a_1$ molecular state of the water molecule. The positron-induced TDCSs (dotted line) clearly appear as smaller in magnitude in comparison to the electron ones (solid line). We also observe that the positron-impact TDCSs show a two-peak structure at the incident energy of 4 eV above IP [Fig. 2(a)], whereas the electron-impact TDCSs show only a broad forward peak at this energy. The experimental TDCSs for the electron-impact case also show a two-peak structure at this energy [solid circles in Fig. 1(a)]. This may be due to the effect of charge on the molecular collision dynamics. At incident energy 10 eV above IP both positron- and electron-impact TDCSs show two-peak structure. However, the positron-impact TDCSs are smaller in magnitude and the peaks are shifted towards higher values of the scattering angle. For the case of electron impact, the MDW and experimental TDCSs also show a two-peak structure at this energy [dotted line and solid circle in Fig. 1(b)]. As projectile energy increases to 20 and 40 eV above IP, the backward peak of positron-impact TDCSs becomes very small in comparison to the electron-impact case while the forward peak shifts towards lower values of scattering angles [Figs. 2(c) and 2(d)]. Thus, significant differences are observed in the trends of TDCSs for electron- and positron-impact ionization of the water molecule in the present investigation.

## IV. CONCLUSIONS

Electron- and positron-impact triply differential cross sections have been presented for the coplanar ionization of the water molecule at the incident electron energies 2, 10, 20, and 40 eV above ionization potential. The current work based on the second-order distorted-wave Born approximation produces a mixed degree of agreement with the experimental data. Besides, in comparison to the rare experimental data available in the literature, the reported TDCSs have shown a reasonable agreement in terms of shape. However, we have also observed important discrepancies when the relative amplitudes of the forward- to the backward-scattering peaks were compared, in particular at the lowest energy (4 eV above IP), where MDW results are in better agreement. Differences in the trends of TDCSs have been observed between the electron- and positron-impact triply differential cross sections under similar kinematical conditions. The present attempt is useful to understand the delicate collision dynamics of water molecule and more theoretical efforts are required to gain a clear understanding of the complex reaction mechanism.

## ACKNOWLEDGMENTS

We thank Professor Andrew James Murray for providing experimental data. P.S. acknowledges support through a scholarship provided by Sir Padampat Singhania University (SPSU) for the research work.

[1] C. Champion, C. Le Loirec, and B. Stosic, Int. J. Radiat. Biol. **88**, 62 (2012).
[2] B. Boudaiffa, P. Cloutier, D. Hunting, M. A. Huels, and L. Sanche, Science **287**, 1658 (2000).
[3] J. Colgan and M. S. Pindzola, Phys. Rev. A **74**, 012713 (2006).
[4] M. Takahashi, N. Watanabe, Y. Khajuria, Y. Udagawa, and J. H. D. Eland, Phys. Rev. Lett. **94**, 213202 (2005).
[5] S. Samarin, O. M. Artamonov, A. D. Sergeant, J. Kirschner, A. Morozov, and J. F. Williams, Phys. Rev. B **70**, 073403 (2004).
[6] M. Vos, S. A. Canney, I. E. McCarthy, S. Utteridge, M. T. Michalewicz, and E. Weigold, Phys. Rev. B **56**, 1309 (1997).
[7] C. Jia, A. Lahmam-Bennani, A. Duguet, L. Avaldi, M. Lecas, and C. Dal Capello, J. Phys. B **35**, 1103 (2002).
[8] S. Bellm, J. Lower, K. Bartschat, X. Guan, D. Weflen, M. Foster, A. L. Harris, and D. H. Madison, Phys. Rev. A **75**, 042704 (2007).
[9] J. Lower and E. Weigold, J. Phys. B **23**, 2819 (1990).
[10] I. Bray, Phys. Rev. Lett. **89**, 273201 (2002).
[11] I. Bray, D. V. Fursa, A. S. Kheifets, and A. T. Stelbovics, J. Phys. B **35**, R117 (2002).
[12] A. S. Kheifets, D. V. Fursa, C. W. Hines, I. Bray, J. Colgan, and M. S. Pindzola, Phys. Rev. A **81**, 023418 (2010).
[13] J. Colgan, M. S. Pindzola, F. Robicheaux, C. Kaiser, A. J. Murray, and D. H. Madison, Phys. Rev. Lett. **101**, 233201 (2008).
[14] G. Purohit, P. Singh, V. Patidar, Y. Azuma, and K. K. Sud, Phys. Rev. A **85**, 022714 (2012).
[15] G. Purohit, V. Patidar, and K. K. Sud, Phys. Scr. **80**, 065301 (2009).
[16] S. Jones, D. H. Madison, and M. Baertschy, Phys. Rev. A **67**, 012703 (2003).

[17] S. Rioual, B. Rouvellou, A. Pochat, J. Rasch, H. R. J. Walters, C. T. Whelan, and R. J. Allan, J. Phys. B: At. Mol. Opt. Phys. **30**, L475 (1997).
[18] X. Zhang, C. T. Whelan, and H. R. J. Walters, J. Phys. B: At. Mol. Opt. Phys. **23**, L173 (1990).
[19] P. Singh, G. Purohit, and V. Patidar, J. Phys. B: At. Mol. Opt. Phys. **46**, 115207 (2013).
[20] K. L. Nixon, A. J. Murray, O. Al-Hagan, D. H. Madison, and C. Ning, J. Phys. B: At. Mol. Opt. Phys. **43**, 035201 (2010).
[21] R. Moccia, J. Chem. Phys. **40**, 2186 (1964).
[22] C. Champion, J. Hanssen, and P.-A. Hervieux, Phys. Rev. A **63**, 052720 (2001).
[23] C. Champion, J. Hanssen, and P.-A. Hervieux, Phys. Rev. A **65**, 022710 (2002).
[24] C. Champion, J. Hanssen, and P.-A. Hervieux, J. Chem. Phys. **117**, 197 (2002).
[25] D. S. Milne-Brownlie, S. J. Cavanagh, B. Lohmann, C. Champion, P.-A. Hervieux, and J. Hanssen, Phys. Rev. A **69**, 032701 (2004).
[26] C. Champion, J. Hanssen, and P.-A. Hervieux, J. Chem. Phys. **121**, 9423 (2004).
[27] J. B. Furness and I. E. McCarthy, J. Phys. B **6**, 2280 (1973).
[28] M. E. Riley and D. G. Truhlar, J. Chem. Phys. **63**, 2182 (1975).
[29] S. J. Ward and J. H. Macek, Phys. Rev. A **49**, 1049 (1994).
[30] X. Zhang, C. T. Whelan, and H. R. J. Walters, J. Phys. B: At. Mol. Opt. Phys. **23**, L509 (1990).